IEEE Access
Multidisciplinary | Rapid Review | Open Access Journal

Received March 1, 2021, accepted March 23, 2021, date of publication March 29, 2021, date of current version April 6, 2021.

Digital Object Identifier 10.1109/ACCESS.2021.3069368

Characterization of a Pixelated Cadmium Telluride Detector System Using a Polychromatic X-Ray Source and Gold Nanoparticle-Loaded Phantoms for Benchtop X-Ray Fluorescence Imaging

SANDUN JAYARATHNA[1], MD FOIEZ AHMED[1], LIAM O'RYAN[2], HEM MOKTAN[1], YONGGANG CUI[3], AND SANG HYUN CHO[1,4]

[1]Department of Radiation Physics, The University of Texas MD Anderson Cancer Center, Houston, TX 77030, USA
[2]Quantum Detectors Ltd., Oxford OX11 0QX, U.K.
[3]Brookhaven National Laboratory, Upton, NY 11973, USA
[4]Department of Imaging Physics, The University of Texas MD Anderson Cancer Center, Houston, TX 77030, USA

Corresponding author: Sang Hyun Cho (scho@mdanderson.org)

This work was supported by the NIH under Award R01EB020658.

ABSTRACT Pixelated semi-conductor detectors providing high energy resolution enable parallel acquisition of x-ray fluorescence (XRF) signals, potentially leading to performance enhancement of benchtop XRF imaging or computed tomography (XFCT) systems utilizing ordinary polychromatic x-ray sources. However, little is currently known about the characteristics of such detectors under typical operating conditions of benchtop XRF imaging/XFCT. In this work, a commercially available pixelated cadmium telluride (CdTe) detector system, HEXITEC (High Energy X-ray Imaging Technology), was characterized to address this issue. Specifically, HEXITEC was deployed into our benchtop cone-beam XFCT system, and used to detect gold Kα XRF photons from gold nanoparticle (GNP)–loaded phantoms. To facilitate the detection of XRF photons, various parallel-hole stainless steel collimators were fabricated and coupled with HEXITEC. A pixel-by-pixel spectrum merging algorithm was introduced to obtain well-defined XRF + scatter spectra with parallel-hole collimators. The effect of charge sharing addition (CSA) and discrimination (CSD) algorithms was also investigated for pixel-level CS correction. Finally, the detector energy resolution, in terms of the full-width at half-maximum (FWHM) values at two gold Kα XRF peaks ($\sim$68 keV), was also determined. Under the current experimental conditions, CSD provided the best energy resolution of HEXITEC ($\sim$1.05 keV FWHM), compared with CSA and no CS correction. This FWHM value was larger (by up to $\sim$0.35 keV) than those reported previously for HEXITEC (at $\sim$60 keV Am-241 peak) and single-crystal CdTe detectors (at two gold Kα XRF peaks). This investigation highlighted characteristics of HEXITEC as well as the necessity for application-specific detector characterization.

INDEX TERMS Pixelated CdTe detector, HEXITEC, x-ray fluorescence, benchtop x-ray fluorescence computed tomography, gold nanoparticles.

I. INTRODUCTION

Benchtop x-ray fluorescence (XRF) computed tomography (XFCT) including XRF mapping is a promising technique for quantitative molecular imaging due to its availability under typical biomedical laboratory setting and economical instrumentation resulting from the use of polychromatic x-ray sources [1]. Most early benchtop XFCT devices used a single-crystal/pixel detector to acquire XRF + scattered photon spectra from the imaging object containing metal probes such as gold nanoparticles (GNPs), which required translation of the detector and/or imaging

The associate editor coordinating the review of this manuscript and approving it for publication was yongqiang Zhao.

object sequentially in steps to obtain a complete set of projection data [1]–[5]. While it served well for establishing the proof of principles for benchtop XFCT, this approach typically leads to excessive x-ray dose and/or scan time during benchtop XFCT imaging sessions. For practical applications of benchtop XFCT such as *in vivo* imaging, therefore, alternative approaches are necessary to satisfactorily address the x-ray dose/scan time issue.

One way to accomplish the aforementioned goal is through parallel acquisition of XRF signals using a 2D array of single-crystal detectors or a pixelated detector. Early experimental investigations provided preliminary insight into the advantages (e.g., reduced XFCT scan time) and disadvantages (e.g., reduced system sensitivity) from using 1D or 2D pixelated photon counting detectors for benchtop XFCT [6]–[8]. Similar advantages and disadvantages were also noted in recent benchtop XFCT/XRF mapping studies of live animals [9], [10] using pixelated photon counting detectors and pinhole collimators. In general, pixelated photon counting detectors used for the aforementioned studies allow for acquisition of XRF + scattered photon spectra in a limited number of broad energy bins (vs. full energy spectra). As a result, the use of such detectors poses some challenge in applying well-established (curve fitting-based) XRF signal extraction algorithms that require more detailed XRF + scattered photons spectra (in finer energy bins) [1]. This type of difficulty typically results in less effective XRF signal extraction, leading to the reduced system sensitivity as seen in the studies mentioned above. In order to further enhance the sensitivity of benchtop XFCT, therefore, it is desirable to adopt a fully-spectroscopic pixelated detector system with higher energy resolution.

Meanwhile, we noted a commercial pixelated detector system that appeared to allow for parallel XRF signal acquisition while meeting the technical requirements, especially in terms of the detector energy resolution, for the latest version of our benchtop cone-beam XFCT system [11]. This detector system, known as HEXITEC (High Energy X-ray Imaging Technology) [12]–[14], is based on a fully-spectroscopic pixelated cadmium telluride (CdTe) detector, and has been successfully used for XRF imaging with monochromatic synchrotron x-rays [15]. A recent study also reported the use of HEXITEC to create a multi-detector array for single-photon imaging applications [16]. While it proposed the use of such a multi-detector array for benchtop XFCT, this study mainly focused on developing a multi-channel readout system, thus providing little information about the suitability of HEXITEC for typical benchtop XFCT imaging. For example, similar to a previous study [12], this study also determined the energy resolution of HEXITEC using monoenergetic spectral lines of radioisotope sources and considerably long data acquisition time (120 min). Evidently, such experimental conditions are less relevant for benchtop XFCT systems developed for biomedical applications (e.g., *in vivo* imaging), because these systems utilize polychromatic x-ray sources in the diagnostic energy range and much shorter data acquisition time (e.g., less than 60 seconds at each projection). Thus, the characteristics of HEXITEC under typical operating conditions of benchtop XFCT systems are currently unknown, necessitating an investigation like the present study, which was conducted with a well-documented experimental benchtop cone-beam XFCT setup and GNP–loaded phantoms [11]. The research outcomes from this study will be essential to guide future development of benchtop XFCT systems adopting HEXITEC or similar pixelated detector systems.

II. METHODS

A. HEXITEC SYSTEM

A commercially available HEXITEC detector system (Quantum Detectors, Oxford, UK) [12]–[14] was used in this investigation. HEXITEC operates at room temperature (without any cryogenic cooling) and can detect x-rays in the energy range of ∼3 to 200 keV. The active area of a 1-mm-thick CdTe sensor has a two-dimensional field of view of 2 cm × 2 cm, consisting of 80 × 80 individual pixels (total 6400) on a 250-μm pitch. Each pixel measures the energy deposited by individual photons, with the final x-ray spectrum in each pixel recorded by summing multiple frames with a frame rate of 9 kHz. Note a frame is the compiled energy-resolved x-ray spectra on a per-pixel basis over 80 × 80 total pixels for a time period of 0.1 ms. When fitted with a CdTe detector, HEXITEC operates at a bias voltage of up to −500 V.

B. EXPERIMENTAL BENCHTOP XFCT SETUP

The major components of our experimental benchtop cone-beam XFCT setup are illustrated in Fig. 1a, which included an irradiation component, a GNP-loaded imaging phantom at the isocenter, and a detection component to detect XRF and scattered x-rays. The irradiation component consisted of an x-ray source with a tungsten target (COMET AG-type MXR-160/22), operating at 125 kVp and 24 mA with a focal spot size of 5.5 mm, coupled to a 5-cm thick lead cone-beam collimator (1-cm inlet diameter and 2-cm outlet diameter), and a 1.8-mm tin filter connected to the collimator outlet [11]. The irradiation component produced a cone-beam with a diameter of ∼3 cm at the imaging isocenter.

The detection component consisted of HEXITEC, placed at 90° with respect to the incident beam direction and inside a custom shielded chamber made of stainless steel, aligned towards the imaging isocenter. The detector could be coupled with either of two 5-cm thick stainless steel parallel-hole collimators drilled with cylindrical apertures. One collimator had a 1-mm diameter aperture at the center (referred to as ''1-mm collimator''), whereas the other collimator had a 2.0-mm diameter aperture at the center (referred to as ''2-mm collimator''). The detection component was installed on a fixed linear stage with an isocenter-to-detector distance of 10 cm so that no horizontal or vertical movements occurred during the data acquisition.

The GNP-loaded phantom used during the basic detector characterization work was a 1-cm diameter cylindrical plastic tube filled with 500 μL of GNP solution at a selected concentration of 1 mg Au/cm^3 (1.0 wt.%)(Fig. 1b). A 3-cm diameter cylindrical acrylic phantom containing three imaging insert slots [11] was also used during the testing of parallel XRF data acquisition (Fig. 1c). For both phantoms, the source-to-imaging isocenter distance was fixed at 15 cm. GNP solution was created using commercially available 15-nm-diameter GNPs (AuroVist, Nanoprobes, Inc.)

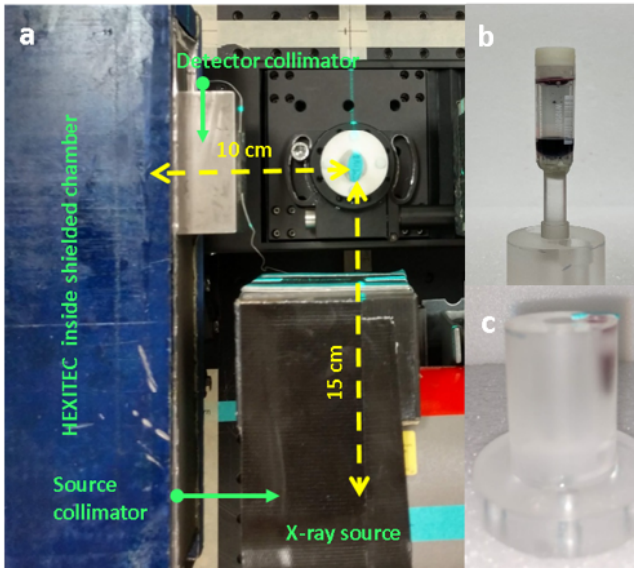

FIGURE 1. (a) Benchtop XRF/XFCT imaging system. A 125 kVp x-ray source, source collimator, imaging phantom, detector collimator and the HEXITEC detector system. (b) GNP-loaded phantom is a 1-cm diameter cylindrical plastic tube filled with 1 mg Au/cm^3 GNP solution. (c) A 3-cm diameter cylindrical acrylic phantom with a GNP-filled insert.

C. DATA ACQUISITION

HEXITEC was controlled via the manufacturer's proprietary acquisition software. Gigabit Ethernet was used for communication between the control PC and the detector. Upon connection with the detector after power-on, the bias voltage of -500 V was applied, and the appropriate data acquisition time was set. The operating temperature of the detector was automatically held at $\sim$27° C during the data acquisition. An energy calibration curve for HEXITEC was obtained following a previous study [12] using two radioisotope sources (Am-241 with a photopeak at 59.5 keV and Co-57 with photopeaks at 122 and 136 keV). This curve was used to convert the channel numbers into appropriate energy bins, and in the current analysis, 800 channels were used over the energy range of 0 to 128 keV with a bin width of 0.16 keV.

After data acquisition was completed, two output files were generated per frame and saved in a user-defined location. The first file (proprietary .hxt file format) was used to read the per-pixel energy spectra after all frames were merged and to visualize the built-in 2D-sensitive detector panel images. The second binary file (.bin) was used to post-process the data for different acquisition modes (normal, charge discrimination or charge addition modes) using the acquisition software.

III. RESULTS

A. BUILT-IN 2D IMAGING FROM THE SENSITIVE AREA OF THE DETECTOR

A useful feature in the user interface of HEXITEC software is the dynamic 2D integral imaging of the sensitive area of the detector during the data acquisition. In the current investigation, we used this feature to further adjust the detector collimator alignment with the imaging phantom. Fig. 2 shows the multi-frame 2D images acquired during the irradiation of the imaging phantom for 60 seconds of integration time (54×10^4 frames) using the 1-mm (Fig. 2a) and 2-mm (Fig. 2b) collimators. In both images, clustered high intensity pixels around the central collimator region (X, Y $\sim$ 40) were clearly visible in the 2D pixel panel. The color bar represents the number of XRF + scattered photons detected by a given pixel over the integrated energy range of 3-128 keV. As observed for the 1-mm collimator, detector pixels were clustered in $\pm$ 3 pixel area, while they were clustered in $\pm$ 5 pixel area for the 2-mm collimator.

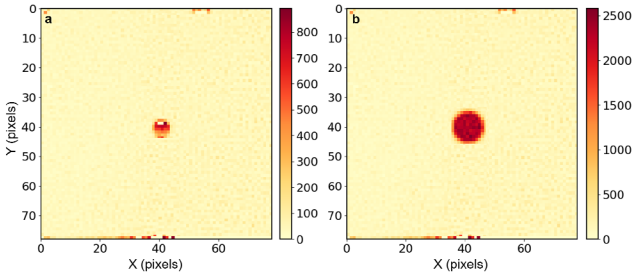

FIGURE 2. Images of the 2D sensitive area of the detector. Zero-degree projection with XRF + scattered photons passed through (a) the 1-mm collimator and (b) the 2- mm collimator. Only one aperture at the center of each collimator was used during the measurements.

B. PER-PIXEL X-RAY SPECTRA

After multiple acquisitions of frames, the per-pixel x-ray energy spectra were extracted using the .hxt file. Given the relatively short data acquisition time (60 seconds), however, it was difficult to acquire statistically stable XRF + scattered photon spectra at the per-pixel level as shown in Fig. 3a (using the 2-mm collimator). As shown for the consecutive pixels [X, Y = 40, 41], [X, Y = 40, 40], and [X, Y = 40, 39], the acquired photon counts were considerably low, which impacted the Compton scatter background fitting and the subsequent net XRF signal extraction [5]. Thus, for more robust spectral data, the data acquisition time was increased by 10 times (600 seconds, $\sim 54 \times 10^5$ frames using the 2-mm collimator; Fig. 3b) while keeping the same experimental conditions. Under this setting, well-defined XRF + scattered photon spectra with two differentiable XRF peaks were detected and enabled the fitting of Compton scattered background and the extraction of net XRF signals. Note the currently chosen data acquisition

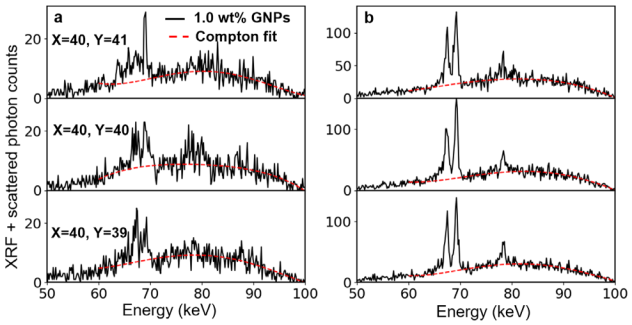

FIGURE 3. Detected XRF + scattered photon spectra in selected consecutive pixels, [X, Y = 40, 41], [X, Y = 40, 40], and [X, Y = 40, 39] obtained using the 2-mm collimator with acquisition time of (a) 60 s, and (b) 600 s.

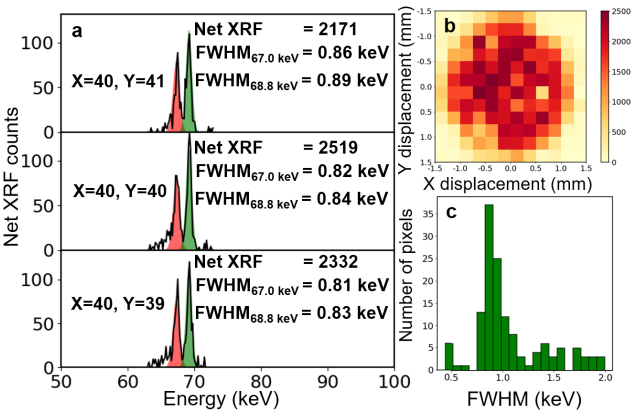

FIGURE 4. (a) The gold Kα XRF peaks and integrated net XRF photon counts in selected consecutive pixels ([X, Y = 40, 41], [X, Y = 40, 40], and [X, Y = 40, 39]) using the 2-mm collimator and 600 s of acquisition time. The peaks at 67.0 and 68.8 keV were fitted with Gaussian function to determine FWHM. (b) Distribution of net XRF counts within the collimated region. (c) Variation of the estimated per-pixel FWHM values for the collimated region at 68.8keV with a mean value of ∼1.01 keV.

time is considered impractical for benchtop XRF/XFCT imaging applications. Nonetheless, it was necessary to evaluate some important detector properties at the per-pixel level (e.g., detector energy resolution, XRF detection efficiency) over gold K-shell XRF energy windows.

Using the spectra obtained with the 2-mm collimator and 600 s of acquisition time, the net XRF signals were extracted by subtracting the fitted scatter background from the detected signal. The full-width at half-maximum (FWHM) values around gold Kα XRF peaks, 67.0 keV (Kα2) and 68.8 keV (Kα1), were determined by fitting the spectra with two Gaussian functions in the range of 60-80 keV centered at the XRF peaks (Fig. 4a). As noted, the integrated net XRF counts in consecutive pixels varied. This is further demonstrated in Fig. 4b, where net XRF counts are tabulated for each pixel in the central collimated region. The color bar represents the number of net XRF photons detected by a given pixel over the integrated energy window of 63-73 keV. Due to the noted variation in the net XRF signals, the estimated per-pixel FWHM values also varied across the pixels in the central collimated region. Nonetheless, at 67.0 or 68.8 keV, similar FWHM values were observed for a given pixel, but substantially different among nearby pixels. As shown in Fig. 4c, the FWHM values at 68.8 keV for the collimated region ranged between 0.5 and 2.0 keV, with an estimated mean value of ∼1.01 keV.

C. PIXEL-BY-PIXEL SPECTRUM MERGING

To avoid long data acquisition time impractical for imaging purpose, a pixel-by-pixel spectrum merging technique was developed to obtain well-defined XRF + scattered photon spectra, in connection with parallel-hole collimators. Specifically, the consecutive spectra in nearby pixels from the central pixel of the appropriate collimator region for 60 s acquisition time were summed with an equal weight in the corresponding energy bins. The corresponding energy spectra for the given pixel regions are shown in Fig. 5a for the 1-mm collimator setup. The merged spectra clearly showed an improvement in statistical fluctuation of the accumulated data as well as in the spectral regions containing the GNP-induced XRF signals (63-73 keV). The same spectra for the 2-mm collimator setup

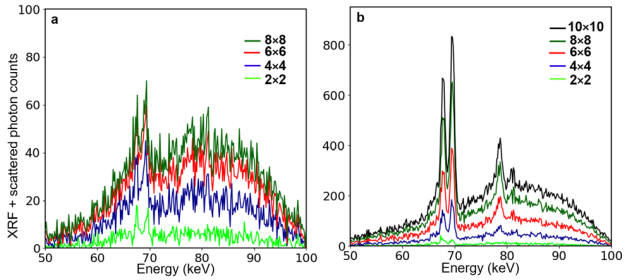

FIGURE 5. Effect of pixel-by-pixel spectrum merging for 60 s acquisition time. Merged energy spectra of the selected pixels (a) for the 1-mm collimator and (b) for the 2-mm collimator showing improved statistical fluctuations and XRF photon detection in the region of interest (63-73 keV).

are shown in Fig. 5b. As shown, the spectrum merging always needed to be performed with the maximum number of pixels corresponding to each collimated detector region (e.g., 8 × 8 and 10 × 10 for the 1-mm and 2-mm collimators, respectively) for the best results.

Due to low photon counts observed during the initial experiment with the 1-mm collimator, a decision was made to proceed with the 2-mm collimator for subsequent experiments in the current investigation. Specifically, the accumulated XRF signal, even after spectrum-merging based on nearby pixels, was considerably lower for the 1-mm collimator as depicted in Figs. 6a and 6b. In this intra-comparison, the y-axis shows the net XRF signals extracted, and the x-axis shows the number of pixels used in the spectrum merging, ranging from 2 × 2 to 8 × 8 in the 1-mm collimator and 2 × 2 to 10 × 10 in the 2-mm collimator. For the 1-mm collimator, there were ∼9 times more net XRF signals from the 8 × 8 pixel-merged spectrum than that from the 2 × 2 pixel-merged spectrum. Similarly, ∼22 times more net XRF signals can be accumulated for the 10 × 10 pixel-merged spectrum, compared to the 2 × 2 pixel-merged spectrum, in the 2-mm collimator.

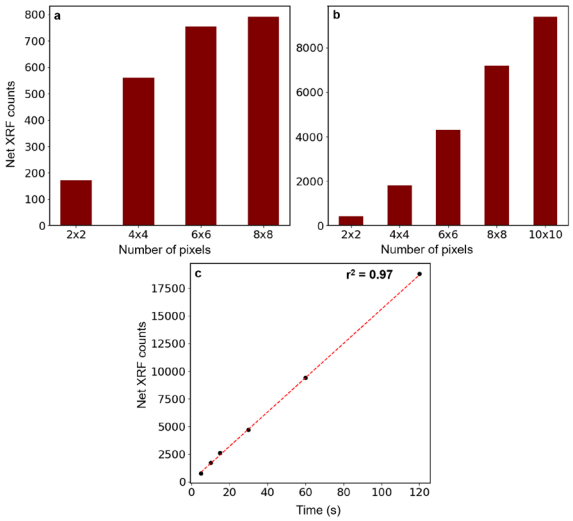

FIGURE 6. Effect of pixel-by-pixel spectrum merging on XRF counts. (a) 1-mm and (b) 2-mm collimators, clearly showing an increase in XRF counts at the same 60 s acquisition time as the number of pixels used for spectrum merging increases. (c) Net XRF counts vs. acquisition time based on the spectrum merging of 10 × 10 pixels for 2-mm collimator, showing the linearity of XRF counts with acquisition time.

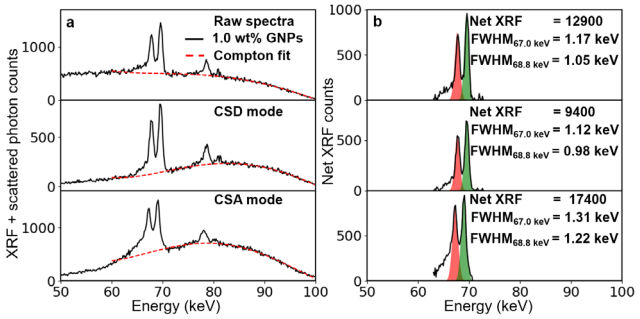

FIGURE 7. Effect of charge-sharing correction algorithms. Raw spectra were obtained using the 2-mm collimator and 60 s of acquisition time. (a) Merged spectra of 10 × 10 pixels for raw data, CSD correction, and CSA correction. (b) Extracted net XRF signal for raw data, after CSA correction, after CSD correction and corresponding FWHM values at energy window of interest after Gaussian fitting.

In Fig. 6c, the net XRF counts for the 2-mm collimator, based on the spectrum merging of 10×10 pixels, were plotted against the acquisition time of 5, 10, 15, 60 and 120 s. The results were fitted with a linear polynomial, showing a high linearity with the Pearson correlation coefficient of $r^2 = 0.97$. This suggested that, under the current experimental condition, the pixel-by-pixel spectrum merging technique was effective in extracting XRF signals across a wide range of acquisition time (per projection) deemed relevant for benchtop XRF/XFCT imaging of biological objects.

D. EFFECT OF CHARGE SHARING ON THE ACQUIRED SPECTRA

In pixelated detectors, there is an effect known as charge sharing, in which multiple pixels share the electron cluster from the same x-ray interaction event. The average size of the charge cluster created by an x-ray interaction in a CdTe crystal was reported to be on the order of $\sim 10\ \mu$m [14], thus the less separation between the neighboring pixels, the higher the probability of the charge sharing effect. To address this issue, HEXITEC offers two correction algorithms for the charge sharing effect: charge sharing discrimination (CSD) and charge sharing addition (CSA) [17], [18]. Fig. 7a shows x-ray spectra obtained by spectrum merging of 10×10 single pixels collected over 60 s of data acquisition time using the 2-mm collimator setup. The x-ray spectra based on raw data (no correction for charge sharing) as well as the data corrected by CSA and CSD are shown in this figure. The extracted net XRF signal corresponding to each of these three spectra is shown in Fig. 7b. The results clearly demonstrated the effect of different correction algorithms applied to the acquired data. Quantitatively, the XRF peak-to-Compton background ratio was $\sim$2.5 with CSA correction and $\sim$5.8 with CSD correction, suggesting significant improvement in the signal-to-noise ratio of the extracted XRF signal by CSD correction. Although it provided a good XRF signal and better energy resolution around gold K α 1 and Kα2 XRF peaks, CSD correction also resulted in reduction of the extracted net XRF signal. In contrast, CSA correction provided larger XRF signal, compared with CSD correction, with a reduction in the observed energy resolution.

E. DETECTOR ENERGY RESOLUTION WITH DIFFERENT CORRECTION ALGORITHMS

After charge sharing correction followed by pixel-by-pixel spectrum merging, their combined effect on the detector energy resolution was investigated quantitatively as illustrated in Fig. 7b. The CSA-corrected spectrum provided the worst detector energy resolution (average FWHM $\sim$1.26 keV) around the 66-69 keV energy window containing two gold XRF peaks (gold Kα1 and Kα2). FWHM values estimated from the CSD-corrected spectrum were 1.12 and 0.98 keV at gold Kα2 and Kα1 peaks, respectively, whereas those based on the raw data were 1.17 and 1.05 keV at the two respective gold Kα XRF peaks. In practice, the average FWHM values of 1.05 and 1.11 keV can be taken as the estimated energy resolution of HEXITEC with and without charge sharing correction at the energy window of interest (66-69 keV) within the spectrum obtained with the 2-mm collimator and 60 s of acquisition time.

F. PARALLEL XRF DETECTION USING HEXITEC

After HEXITEC was tested for its operating characteristics under the current experimental conditions, its ability for parallel XRF detection was also investigated by using one-dimensional parallel-hole stainless steel collimator that had seven parallel-holes of 2.0-mm diameter with 1.0-mm septal thickness (Fig. 8a). The collimator was fabricated in such a way that the holes covered the 2-cm field of view of the detector. For this task, a GNP-filled Eppendorf tube was inserted into a 3-cm diameter cylindrical acrylic phantom as

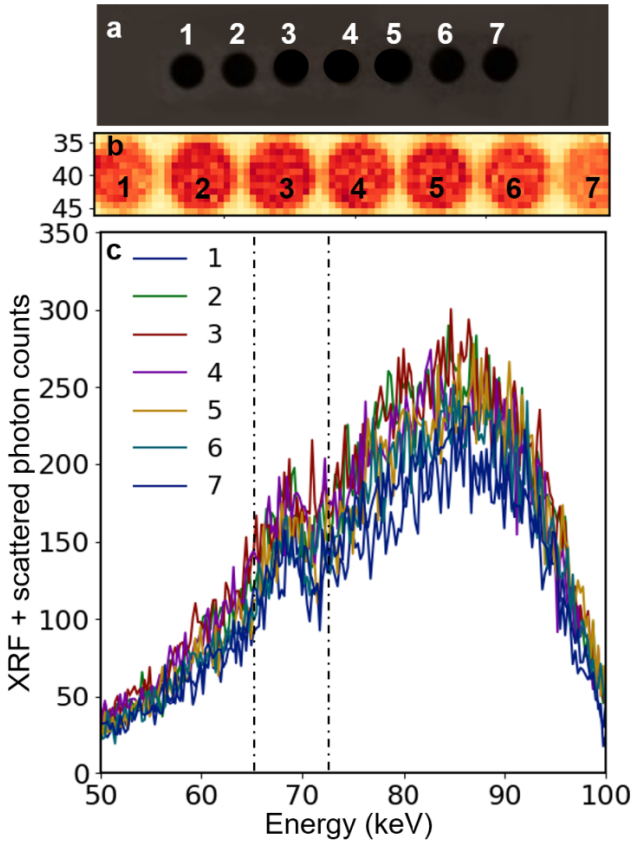

FIGURE 8. Parallel acquisition of photon spectra using HEXITEC for 60s acquisition time. (a) Parallel-hole collimator with 7 holes (2-mm hole diameter) with 1-mm septal thickness. (b) Zero-degree projection with XRF + scattered photons passed through the parallel-hole collimator. (c) XRF + scattered photon spectrum corresponding to each collimated region after spectrum merging of 10 × 10 single pixels. The dashed line illustrates the region of spectral interest (63-73 keV).

shown earlier (Fig. 1c). The multi-frame 2D image of the sensitive area acquired during the irradiation of the phantom for 60 s is shown in Fig. 8b. As depicted, all parallel collimator holes were clearly visible along the central row ($y \sim 40$) of the 2D pixel panel. The edges of the collimated regions were not overlapped and well separated due to the selected collimator septum of 1 mm. XRF + scattered photons spectra (after spectrum merging of 10 × 10 single pixels) acquired through seven parallel-hole collimators are shown in Fig. 8c, demonstrating the feasibility of acquiring spectral data in parallel using the current setup. To obtain the same number (7) of spectra with a single crystal detector, the detector would have to be translated 6 times along the horizontal direction, requiring a total acquisition time of 420 s ($= 7 \times 60$ s).

IV. DISCUSSION

One of the key technological challenges in the development of practical benchtop XRF/XFCT imaging systems has been the lack of x-ray imaging detectors suitable for benchtop XRF/XFCT imaging. The focus of the current investigation was therefore to delineate the strengths and weaknesses of HEXITEC, a commercially available 2D pixelated spectroscopic detector, which appears to meet the minimum technical specifications required for benchtop XRF/XFCT imaging. In essence, the current study represents the first-time testing, to the best of our knowledge, of HEXITEC in an ordinary polychromatic x-ray beam line to detect XRF photons emitted by GNPs. The performance of HEXITEC for XRF applications was demonstrated previously under the monochromatic synchrotron x-ray environment [15], [19]. On the other hand, little is known at this time regarding its performance under the benchtop setting where the use of polychromatic diagnostic energy range x-ray sources (e.g., tube voltages > 100 kVp) results in more pronounced scatter background, introducing additional complexity in detection/extraction of XRF signals.

Besides the characterization of HEXITEC, the current investigation provided insight into the use of parallel-hole detector collimators coupled with 2D pixelated spectroscopic detectors under the cone-beam geometry. Over the years, the current research team has demonstrated the feasibility of this setup by Monte Carlo simulations [20]–[22] and experimental investigations (where single crystal detectors and detector translations were combined to mimic such a setup)[2], [11], while attempting to address the x-ray dose/scan time issue that holds the key for routine *in vivo* XRF/XFCT imaging with benchtop systems. Due to the nature of previous studies, however, it has been difficult to provide a realistic outlook about the operating characteristics of such a system. For example, the necessity or the degree of complexity to apply a pixel-by-pixel spectrum merging technique was hard to discern from previous studies. As shown in the current investigation, this technique plays an essential role for obtaining well-defined XRF + scattered photon spectra with parallel-hole collimators within the given time constraint, thereby potentially reducing the x-ray dose/scan time.

Furthermore, the current investigation determined the effects of important technical issues associated with pixelated detectors, such as charge sharing and detector energy resolution, within the context of benchtop XRF/XFCT imaging, which was not possible in previous studies by the current team and other groups. The results suggest that, under the current experimental conditions with HEXITEC, CSD correction algorithm can be used to further improve the XRF signal-to-noise ratio. On the other hand, CSA correction could be preferred for typical XRF/XFCT applications because of its ability to increase the overall efficiency of the detector (for example, by providing about two times more XRF signal, compared with CSD correction). Regarding the detector energy resolution, HEXITEC provided larger average FWHM values (e.g., 1.05 keV with CSD correction and 1.11 keV with no correction) around gold Kα XRF peaks (the energy range of 67–69 keV), compared with a commercial single crystal CdTe detector (manufactured by Amptek) that provides an estimated 0.7 keV FWHM around the same gold Kα XRF peaks according to a previous study [11] performed with the same benchtop XFCT setup, GNP-loaded phantom,

and irradiation geometry/parameters, as used in the current study. Based on measurements with a radioisotope source (Am-241 peak at 59.5 keV), a previous study reported a comparable energy resolution between HEXITEC and Amptek CdTe detectors across a similar x-ray energy range [12]. A recent study, which also used the same radioisotope source, reported an energy resolution of 0.8 keV FWHM for HEXITEC [16]. As demonstrated in the present study, however, the energy resolution of HEXITEC was further degraded under the current experimental conditions: most notably, relatively high energy/polychromatic incident x-ray spectrum resulting in large Compton scatter background below the XRF peaks as well as more pronounced charge sharing effect; relatively short data acquisition time and collimated detector pixels leading to inferior photon counting statistics. Thus, it is critical to characterize HEXITEC under the operation conditions most relevant to specific applications (e.g., GNP-based benchtop XFCT imaging). Moreover, any considerable degradation of the detector energy resolution (e.g., by a magnitude similar to that reported in this study) may have to be carefully taken into account during the design of a benchtop XFCT system, as it will likely prevent the developed system from meeting the technical requirements (e.g., sensitivity) for specific applications. For benchtop XFCT imaging of GNP-containing objects, a deconvolution-based XRF signal extraction algorithm, developed in our previous study [21], can be used to mitigate potential consequences of the reduced energy resolution of HEXITEC or similar pixelated detector systems.

V. CONCLUSION

In the current investigation, we examined the performance of a fully-spectroscopic pixelated CdTe detector system, HEXITEC, for detecting gold Kα XRF photons emitted from GNP-containing phantoms using our benchtop cone-beam XFCT setup. We found that HEXITEC, in conjunction with appropriate detector collimators, allowed for parallel acquisition of x-ray (XRF + scattered) spectra, which is considered necessary for more efficient benchtop XRF/XFCT imaging. Regardless of the aperture size (1- or 2-mm diameter) in parallel-hole detector collimators, x-ray spectrum scored by each detector pixel within the collimated region must be merged to provide statistically stable XRF signal suitable for imaging purpose. After pixel-by-pixel spectrum merging, CSD algorithm, compared with CSA algorithm and no CS correction, provided the best energy resolution of $\sim$1.05 keV FWHM around two gold Kα XRF peaks (the energy range of 67–69 keV). This FWHM value was larger than the value (0.7 keV FWHM) quoted for a commercially available (Amptek) single crystal CdTe detector in a published study performed with the same benchtop XFCT setup, GNP-loaded phantom, and irradiation geometry/parameters, as used in the current study. The aforementioned FWHM value of HEXITEC ($\sim$1.05 keV) was also larger than the values (0.8-1 keV FWHM) previously determined with radioisotope sources (using the Am-241 peak at $\sim$60 keV). This finding strongly suggested the energy resolution of HEXITEC would vary dependent on experimental conditions. Thus, HEXITEC needs to be characterized under the operation conditions most relevant to specific applications. Overall, the results and findings from this study, as highlighted above, should be taken into account for the design of a benchtop XRF/XFCT system adopting HEXITEC or similar pixelated detector systems.

ACKNOWLEDGMENT

The authors would like to thank Ms. Erica Goodoff from Scientific Publications with The University of Texas MD Anderson Cancer Center for editorial assistance with the manuscript.

REFERENCES

[1] S. K. Cheong, B. L. Jones, A. K. Siddiqi, F. Liu, N. Manohar, and S. H. Cho, "X-ray fluorescence computed tomography (XFCT) imaging of gold nanoparticle-loaded objects using 110 kVp X-rays," *Phys. Med. Biol.*, vol. 55, no. 3, p. 647, Jan. 2010.

[2] B. L. Jones, N. Manohar, F. Reynoso, A. Karellas, and S. H. Cho, "Experimental demonstration of benchtop X-ray fluorescence computed tomography (XFCT) of gold nanoparticle-loaded objects using lead- and tin-filtered polychromatic cone-beams," *Phys. Med. Biol.*, vol. 57, no. 23, pp. N457–N467, Dec. 2012.

[3] Y. Kuang, G. Pratx, M. Bazalova, B. Meng, J. Qian, and L. Xing, "First demonstration of multiplexed X-ray fluorescence computed tomography (XFCT) imaging," *IEEE Trans. Med. Imag.*, vol. 32, no. 2, pp. 262–267, Feb. 2013.

[4] Y. Kuang, G. Pratx, M. Bazalova, J. Qian, B. Meng, and L. Xing, "Development of XFCT imaging strategy for monitoring the spatial distribution of platinum-based chemodrugs: Instrumentation and phantom validation," *Med. Phys.*, vol. 40, no. 3, Feb. 2013, Art. no. 030701.

[5] N. Manohar, F. J. Reynoso, P. Diagaradjane, S. Krishnan, and S. H. Cho, "Quantitative imaging of gold nanoparticle distribution in a tumor-bearing mouse using benchtop X-ray fluorescence computed tomography," *Sci. Rep.*, vol. 6, no. 1, Feb. 2016, Art. no. 22079.

[6] L. Ren, D. Wu, Y. Li, W. R. Chen, B. Zheng, and H. Liu, "Optimized acquisition time for X-ray fluorescence imaging of gold nanoparticles: A preliminary study using photon counting detector," *Proc. SPIE*, vol. 9709, Mar. 2016, Art. no. 97090p.

[7] C. Yoon, Y. Kim, and W. Lee, "3D non-destructive fluorescent X-ray computed tomography with a CdTe array," *IEEE Trans. Nucl. Sci.*, vol. 63, no. 3, pp. 1844–1853, Jun. 2016.

[8] L. Li, S. Zhang, R. Li, and Z. Chen, "Full-field fan-beam X-ray fluorescence computed tomography with a conventional X-ray tube and photon-counting detectors for fast nanoparticle bioimaging," *Opt. Eng.*, vol. 56, no. 4, Apr. 2017, Art. no. 043106.

[9] S. Zhang, L. Li, J. Chen, Z. Chen, W. Zhang, and H. Lu, "Quantitative imaging of Gd nanoparticles in mice using benchtop cone-beam X-ray fluorescence computed tomography system," *Int. J. Mol. Sci.*, vol. 20, no. 9, p. 2315, May 2019.

[10] S. Jung, T. Kim, W. Lee, H. Kim, H. S. Kim, H.-J. Im, and S.-J. Ye, "Dynamic *in vivo* X-ray fluorescence imaging of gold in living mice exposed to gold nanoparticles," *IEEE Trans. Med. Imag.*, vol. 39, no. 2, pp. 526–533, Feb. 2020.

[11] N. Manohar, F. J. Reynoso, and S. H. Cho, "Technical note: A benchtop cone-beam X-ray fluorescence computed tomography (XFCT) system with a high-power X-ray source and transmission CT imaging capability," *Med. Phys.*, vol. 45, no. 10, pp. 4652–4659, Oct. 2018.

[12] P. Seller, S. Bell, R. J. Cernik, C. Christodoulou, C. K. Egan, J. A. Gaskin, S. Jacques, S. Pani, B. D. Ramsey, C. Reid, P. J. Sellin, J. W. Scuffham, R. D. Speller, M. D. Wilson, and M. C. Veale, "Pixellated Cd(Zn)Te high-energy X-ray instrument," *J. Instrum.*, vol. 6, no. 12, Dec. 2011, Art. no. C12009.

[13] M. C. Veale, S. J. Bell, P. Seller, M. D. Wilson, and V. Kachkanov, "X-ray micro-beam characterization of a small pixel spectroscopic CdTe detector," *J. Instrum.*, vol. 7, no. 7, Jul. 2012, Art. no. P07017.

[14] M. C. Veale, P. Seller, M. Wilson, and E. Liotti, "HEXITEC: A high-energy X-ray spectroscopic imaging detector for synchrotron applications," *Synchrotron Radiat. News*, vol. 31, no. 6, pp. 28–32, Nov. 2018.
[15] M. D. Wilson, T. Connolley, I. P. Dolbnya, P. S. Grant, E. Liotti, A. Lui, A. Malandain, K. Sawhney, P. Seller, and M. C. Veale, "Energy dispersive detector for white beam synchrotron X-ray fluorescence imaging," *AIP Conf. Proc.*, vol. 1741, no. 1, 2016, Art. no. 050008.
[16] E. M. Zannoni, M. D. Wilson, K. Bolz, M. Goede, F. Lauba, D. Schöne, J. Zhang, M. C. Veale, M. Verhoeven, and L.-J. Meng, "Development of a multi-detector readout circuitry for ultrahigh energy resolution single-photon imaging applications," *Nucl. Instrum. Methods Phys. Res. A, Accel. Spectrom. Detect. Assoc. Equip.*, vol. 981, Nov. 2020, Art. no. 164531.
[17] M. C. Veale, S. J. Bell, D. D. Duarte, A. Schneider, P. Seller, M. D. Wilson, and K. Iniewski, "Measurements of charge sharing in small pixel CdTe detectors," *Nucl. Instrum. Methods Phys. Res. A, Accel. Spectrom. Detect. Assoc. Equip.*, vol. 767, pp. 218–226, Dec. 2014.
[18] S. L. Bugby, K. A. Koch-Mehrin, M. C. Veale, M. D. Wilson, and J. E. Lees, "Energy-loss correction in charge sharing events for improved performance of pixellated compound semiconductors," *Nucl. Instrum. Methods Phys. Res. A, Accel. Spectrom. Detect. Assoc. Equip.*, vol. 940, pp. 142–151, Oct. 2019.
[19] E. Liotti, A. Lui, T. Connolley, I. P. Dolbnya, K. J. S. Sawhney, A. Malandain, M. D. Wilson, M. C. Veale, P. Seller, and P. S. Grant, "Mapping of multi-elements during melting and solidification using synchrotron X-rays and pixel-based spectroscopy," *Sci. Rep.*, vol. 5, no. 1, Dec. 2015, Art. no. 15988.
[20] B. L. Jones and S. H. Cho, "The feasibility of polychromatic cone-beam X-ray fluorescence computed tomography (XFCT) imaging of gold nanoparticle-loaded objects: A Monte Carlo study," *Phys. Med. Biol.*, vol. 56, no. 12, p. 3719, May 2011.
[21] M. F. Ahmed, S. Yasar, and S. H. Cho, "A Monte Carlo model of a benchtop X-ray fluorescence computed tomography system and its application to validate a deconvolution-based X-ray fluorescence signal extraction method," *IEEE Trans. Med. Imag.*, vol. 37, no. 11, pp. 2483–2492, Nov. 2018.
[22] H. Moktan, M. F. Ahmed, S. Jayarathna, L. Deng, and S. H. Cho, "Monte Carlo study of X-ray detection configurations for benchtop X-ray fluorescence computed tomography of gold nanoparticle-loaded objects," *Phys. Med. Biol.*, vol. 65, Sep. 2020, Art. no. 175010.

SANDUN JAYARATHNA received the Ph.D. degree in high energy particle physics from The University of Houston, Houston, TX, USA, in 2015. His Ph.D. work was in collaboration with the ALICE experiment at CERN, Geneva, Switzerland. After his Ph.D., he worked as a Postdoctoral Fellow and a Research Engineer with The University of Texas MD Anderson Cancer Center, Houston. He is currently working as a Resident Medical Physicist with The University of Kansas Medical Center, Kansas City, KA, USA.

MD FOIEZ AHMED received the Ph.D. degree in photonics from Oklahoma State University, Stillwater, Ok, USA, in 2016. He was a Postdoctoral Fellow with The University of Texas MD Anderson Cancer Center. He is currently working as a Product Physicist with Sun Nuclear Corporation, Melbourne, FL, USA.

LIAM O'RYAN received the Ph.D. degree in structural biology from The University of Manchester, Manchester, U.K., in 2009. He is currently working as a Research and Development Manager with Quantum Detectors Ltd., Oxford, U.K.

HEM MOKTAN received the Ph.D. degree in biophysics from Oklahoma State University, Stillwater, Ok, USA, in 2017. He is currently a Postdoctoral Fellow with The University of Texas MD Anderson Cancer Center, Houston, TX, USA.

YONGGANG CUI received the Ph.D. degree in nuclear technology and application from Tsinghua University, Beijing, China, in 2001. He is currently working as an Electrical Engineer with the Brookhaven National Laboratory, Upton, NY, USA.

SANG HYUN CHO received the Ph.D. degree in nuclear engineering/medical physics from Texas A&M University, College Station, TX, USA, in 1997. He is currently a Professor of radiation physics and imaging physics with The University of Texas MD Anderson Cancer Center, Houston, TX, USA.